Ordering of Binary Colloidal Crystals by Random Potentials
Supplemental Material

André S. Nunes,[1,*] Sabareesh K. P. Velu,[2,*] Iryna Kasianiuk,[3] Denis Kasyanyuk,[3] Agnese Callegari,[3] Giorgio Volpe,[4] Margarida M. Telo da Gama,[1] Giovanni Volpe,[2,5] and Nuno A. M. Araújo[1,†]

[1] *Centro de Física Teórica e Computacional and Departamento de Física, Faculdade de Ciências, Universidade de Lisboa, P-1749-016 Lisboa, Portugal, EU*
[2] *Department of Physics, Bilkent University, Cankaya, 06800 Ankara, Turkey*
[3] *Department of Physics, Bilkent University and UNAM, Cankaya, 06800 Ankara, Turkey*
[4] *Department of Chemistry, University College London, 20 Gordon Street, London WC1H 0AJ, United Kingdom, EU*
[5] *Department of Physics, University of Gothenburg, 41296 Gothenburg, Sweden, EU*

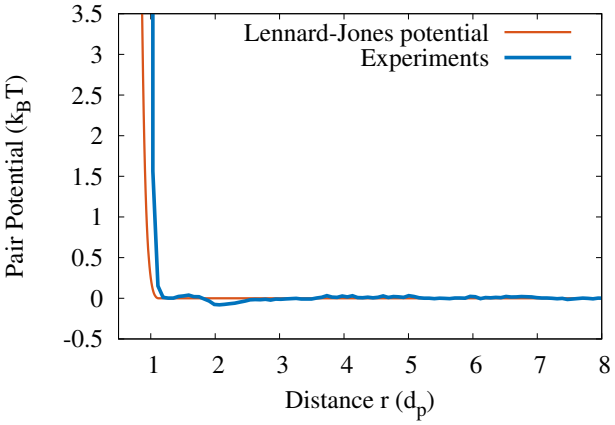

Supplementary Figure S1. Effective interaction potential between pairs of particles in experiments (blue) and the Lennard-Jones potential used in the simulations. The potential is in units of k_BT and the distance r in units of the particle diameter.

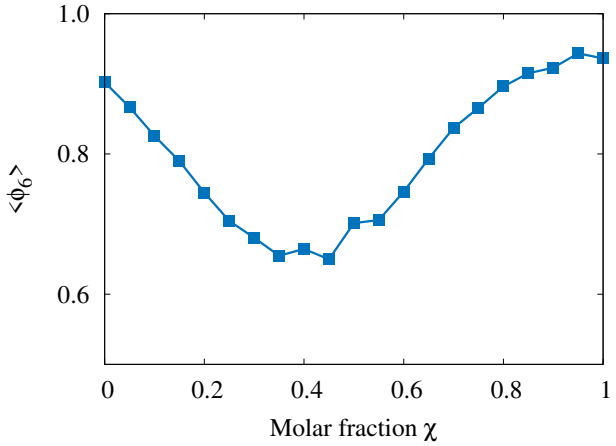

Supplementary Figure S2. Bond order parameter curve in a system where particle-particle interactions are modeled with a Yukawa potential. Parameters: $\sigma = 0.5$, $V = 11.3$ and $V_G/V = 2$, which are condition similar to the one from Fig. 2.

PARTICLE-PARTICLE INTERACTIONS

We followed the procedure to calculate the pairwise interaction potential between particles based on the two-point correlation function [1]. As shown in the Fig. S1, the interactions are essentially repulsive and the potential decays rapidly with the distance, being negligible for values of the distance close to the diameter of the particle. This suggest that, for particles of the size considered here, the interactions are well described by hard-sphere potentials. To avoid the classical numerical problems of dealing with hard spheres (and discontinuous forces) in the simulations, we considered a Lennard-Jones potential that also decays rapidly.

However, in colloidal suspensions the particle-particle interactions are often long ranged, in which case they can be described with a Yukawa potential.

$$V_{ij}(r) = \epsilon \frac{\exp\left(-\frac{r-d_p}{d_p}\right)}{r-d_p}. \quad (1)$$

To show that the non-monotonic dependence of the bond order parameter on the molar fraction of strong particles is a robust result that only requires a repulsive interaction between particles we performed new simulations where we modeled the particle-particle interaction with a Yukawa potential. As shown in the Fig. S2, we obtained the same qualitative result. Note that in these simulations the ratio of response strength to the external potentials between strong and weak particles is four.

PARTICLE HEIGHTS IN THE EXPERIMENTS

To calculate the gravitational height of each colloidal species, we need to account for the balance of four different forces: weight, buoyancy, optical forces, and elec-

	Characteristics of PS particles	Characteristics of Si particles
Surface charge	anionic	anionic
Refractive index	1.59	1.4
Density	1.05 g/cm^3	1.85 g/cm^3
Diameter	6.24 μm	6.73 μm
F optical (ray optics)	35×10^{-3} pN	9×10^{-3} pN

TABLE I. Parameters of the particles in the experiments.

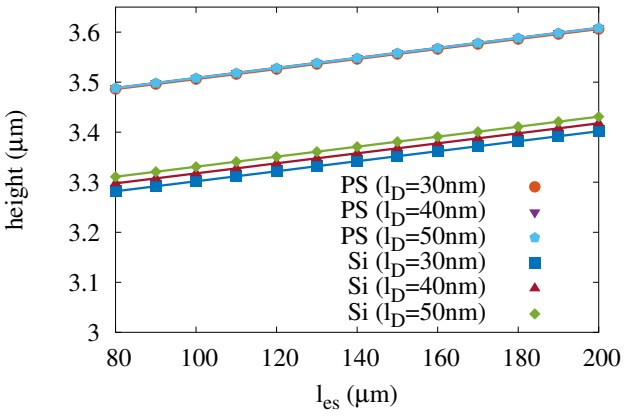

Supplementary Figure S3. Gravitational height of both species calculated with different parameters from Eq. 2.

trostatic forces. The net force should vanish, so the electrostatic repulsive interaction with the glass substrate (pre-cleaned with NaOH to make it hydrophilic) should balance the sum of weight, buoyancy, and optical forces. We express the electrostatic force as [2]

$$F_{es}(d) = -\nabla U_{es}(d) = \frac{k_B T}{l_D} \exp\left(-\frac{d - l_{es}}{l_D}\right), \qquad (2)$$

where d is the distance between the surface of the particle and the substrate, l_D is the Debye length, and l_{es} is a characteristic length. In our case we can assume that the value of l_D is in the range 30 to 60 nm, as estimated from an experiment with silica particles in distilled water. Thus, the pre-factor $k_B T/l_D \approx 0.14 - 0.07$ pN. We also assume that the value of $l_{es} \approx 100 - 200$ nm, slightly bigger than the value found for water-lutidine for silica (90 nm) [3], as distilled water is more polar.

The parameters for the two particle species are summarized in Table I. Figure S3 shows the estimated gravitational height as a function of l_{es}, in the range $80 - 220$ nm, for four different values of l_D, considering a water refractive index of 1.33 and density of 1.00 g/cm^3. In all cases, we find that the gravitational heights for both particle species differ by less than 3% of the particle diameter, suggesting that bidispersity effects resulting from differences in gravitational height are negligible. With such a small difference in gravitational height is very unlikely that one particle would go on top of another and the system can be considered purely two dimensional.

STRENGTH OF THE OPTICAL TRAPS

To verify that, experimentally, the optical potential is strong enough to trap the strong particles but not the weak ones, we analyzed the trajectories of individual particles in the dilute regime. More precisely, we chose a few particles that, during their trajectory in the initial part of the experimental acquisition, showed to have some accumulation point, i.e., each particle in its trajectory spend a few minutes by staying in approximately the same position, without being stuck.

We manually selected those points and, for a quantitative analysis, we take the relevant part of the trajectory near that point and apply the FORMA method [4] which is a method based on a maximum-likelihood-estimator analysis, and it is able to estimates accurately the conservative and non-conservative components of a force field acting on a Brownian particle from the analysis of its displacements. We obtained for Silica particles (weak) and PS particles (strong), respectively, $k_{\text{weak}} = 5fN/\mu m$ and $k_{\text{strong}} = 11fN/\mu m$. This result suggests that the stiffness of the strong particles in the minima is approximately two times higher than that of the weak particles.

We also measured the average modulus of the force acting on each particle due to the speckle, over the entire domain. Using geometrical optics in the experimental speckle profile [5], we obtained $F_{\text{weak}} = (9.36 \pm 4.75)fN$ and $F_{\text{strong}} = (18.87 \pm 9.63)fN$, and for the simulations, $F_{\text{weak}} = (5.81 \pm 4.21)fN$ and $F_{\text{strong}} = (11.61 \pm 8.44)fN$. Thus, we obtain the same order of magnitude of the forces and, more importantly, a similar ratio between the average forces for strong and weak particles.

COMMENT ON PARTICLE BIDISPERSITY

We preformed a set of experiments with binary solutions that was carried out to determine if bidispersity influences the measurements of the bond order parameter. We modified the setup by attaching a mechanical oscillator to a part of the multimode fiber. The vibra-

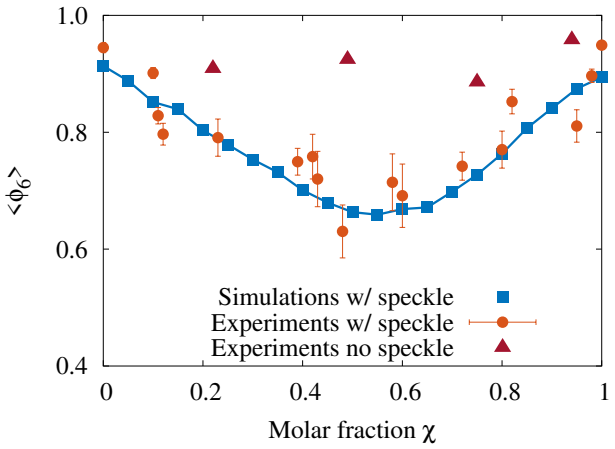

Supplementary Figure S4. Six-fold bond order parameter $\langle\phi_6\rangle$ as a function of the molar fraction χ obtained experimentally with the particles subject only to a Gaussian envelope (triangles) and with the speckle for the experiments (circles) and the simulations (squares).

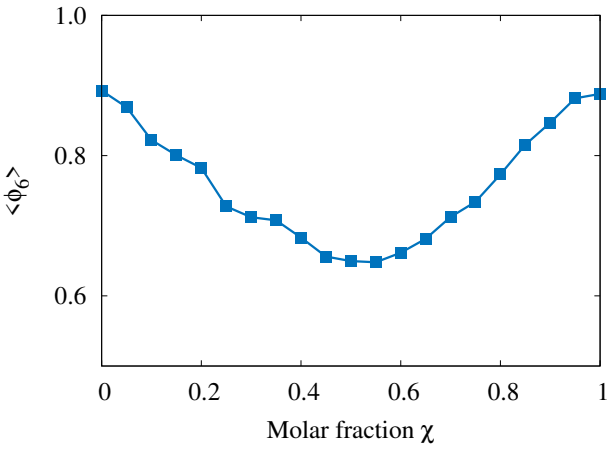

Supplementary Figure S5. Bond order parameter curve for higher densities also displays a minimum. Parameters: $\sigma = 0.5$, $V = 11.3$ and $V_G/V = 0.67$.

tional frequency could be adjusted with DC voltage and increased up to 12000 rpm. By turning the oscillator on, we were able to generate a smooth speckle pattern and create an optical field where the statistical properties of the speckle are averaged out. This way, we were able to create a smoothed pattern. The bond order parameter depends strongly on the presence of strong particles under the speckle field, as seen in Fig.2. However, with a smooth potential we observed the formation of a crystal-like structures with bond order parameter in the range $0.9 - 0.97$, for all χ values (see Fig. S4). As such, we can confidently conclude that bidispersity does not affect our measurements.

HIGH DENSITIES

In Fig. S5 we show the bond order parameter in a system with 25% more particles than the simulations shown in the rest of the paper. Even for higher densities the curve displays a clear minimum and the rearrangement of the structure for higher molar fractions also occurs, showing that this phenomenon is robust to considerable changes in the total density.

VORONOI CELL SIZE

Figure S6 shows the average Voronoi-cell area of the experiments and simulations from Fig. 2 in the main paper. We find that the Voronoi-cell size are does not vary significantly as χ changes compared with the particle size.

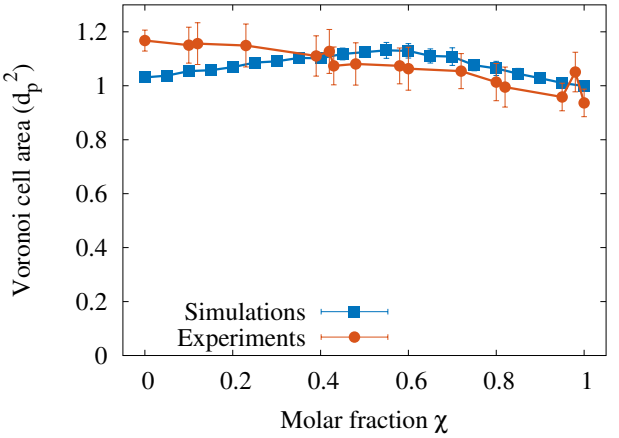

Supplementary Figure S6. Average Voronoi cell area for the experiments (orange circles) and the simulations (blue squares) in Fig. 2.

PARTICLE DIFFUSION IN THE SPECKLE FIELD

We measured the particle's mean square displacement at late times in our simulations ($t > 1.5 \times 10^3 \tau$) and estimated the diffusion coefficient, D, from a linear fit of the time dependence of the mean square displacement. As can be seen in Fig. S7, the strong particles diffuse less than the weak ones, as they get trapped in the local minima of the random potential. Comparing these plots with Fig. 4, we find that higher diffusion coefficients correspond to lower $\langle\phi_6\rangle$, when more defects are formed and the particles' packing is lower.

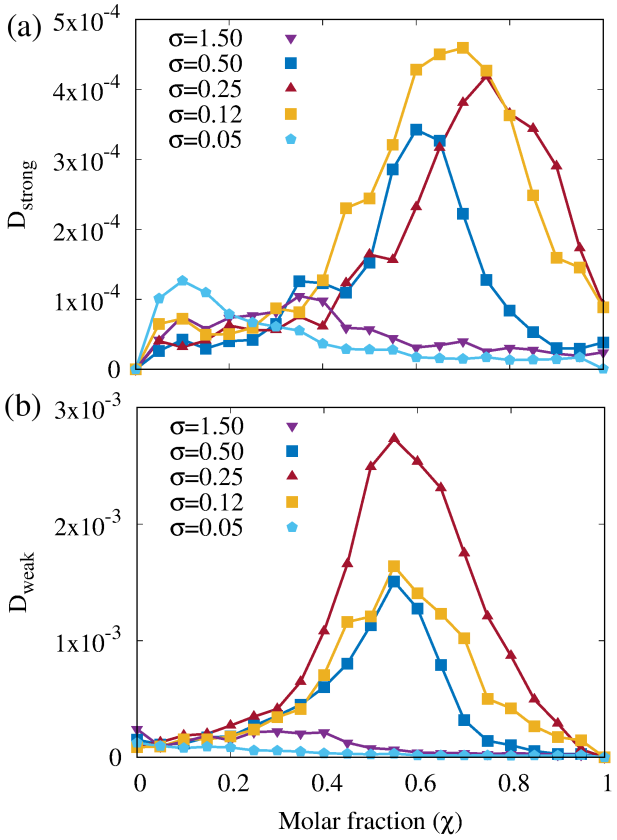

Supplementary Figure S7. (a) Strong and (b) weak particle diffusivity at late times in the same simulations as those shown in Fig. 4. The diffusivity is in units of $d_p^2\tau^{-1}$.

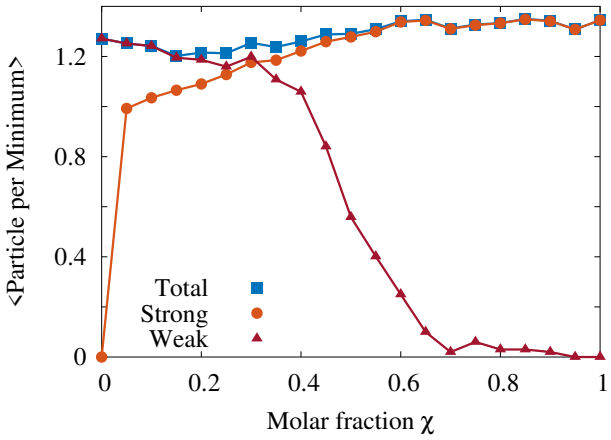

Supplementary Figure S8. Number of particles per speckle peak as a function of the molar fraction in simulations. The total number of particles is represented by the blues line, the strong particles by the orange line and the weak by the red line. These results were obtained from the simulations shown in Fig. 2 from the main paper.

PARTICLE DISTRIBUTION AT THE SPECKLE INTENSITY PEAKS

We counted also the number of strong and weak particles situated in minima of the random potential as a function of χ. As shown in Fig. S8, the minima are mainly populated by strong particles and the average number of particles is higher for values of χ above the value where the six-fold bond order parameter is minimal.

To compute this calculation, we set a threshold to define the boundaries of the speckle minima to be at 15% of the maximum intensity. Note that since the intensities are exponentially distributed the total area of the regions we are considering correspond to $\sim 20\%$ of the area of the system (we tried different thresholds and the results are qualitatively similar). The total number of particles averaged over 100 samples remains constant as a function of the molar fraction and there are, on average, more than one particle in the regions defined by the threshold.

EFFECTIVE SPECKLE PROPERTIES

We are interested in the limit where the dispersion in the speckle correlation function, σ, is of the same order as the particle size or smaller. Thus, to calculate the speckle-induced forces acting on a particle, we need to consider all intensities over the particle's cross-section. We can determine an effective speckle that, at each point, is the average intensity of the original speckle over a particle cross-section. This operation, smooths out the roughness of the intensity surface. This effect can be seen in Fig. S9, where it is clearly shown that the integration decreases the height of the intensity minima and increases the value of the lower intensity regions.

The statistical properties of the effective speckle are different from those of the original one. Figure S10 shows a comparison between the intensity distributions for different σ (histograms) and the original one (dashed line). For high σ, the averaging eliminates the highest intensities but hardly affects the distribution otherwise, as it remains approximately exponential. However, for lower σ, both high and low intensities are eliminated and the distribution is considerably affected. For the lowest σ, the intensities are narrowly distributed around a well-defined value.

The shape of the Gaussian intensity correlations also changes with the averaging. In particular, their dispersions increase. Figure S11 shows the dispersion of the correlations in the effective speckle, σ_{eff}, as a function of the standard deviation of the original speckle, σ. The dashed line corresponds to $\sigma_{\text{eff}} = \sigma$. For higher σ, the averaging does not change the dispersion significantly, because in this limit the features of the surface are, on av-

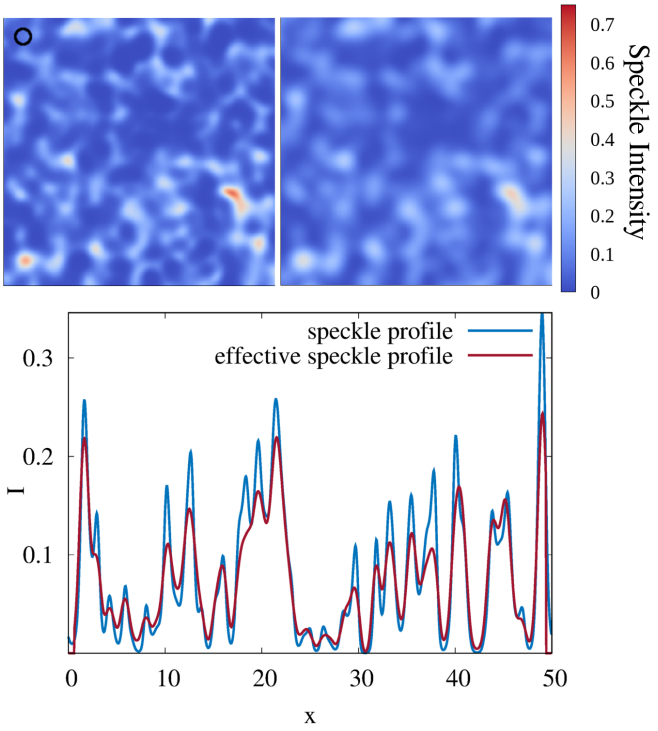

Supplementary Figure S9. Top left, the original speckle intensity surface; the black circle indicates the particle size. Top right, the effective speckle where each intensity point is an average of the intensities of the original one. Bottom, profile of the intensity surface of the original (blue) and the effective speckle (red) for $\sigma = 0.5$. The maximum speckle intensity is defined as the unit of intensity.

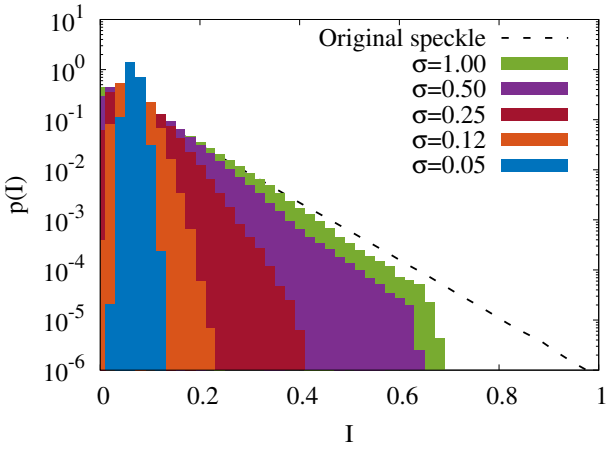

Supplementary Figure S10. Distribution of the speckle intensities of the effective speckles. 100 samples were used for each distribution. The dashed line corresponds to the original intensity distribution, for reference. The maximum speckle intensity is defined as the unit of intensity.

erage, larger than the particle size. For decreasing σ, σ_{eff} increases with respect to the original value, the speckle minima become wider and shallower, which leads to a lower effective force induced by the speckle on the particles.

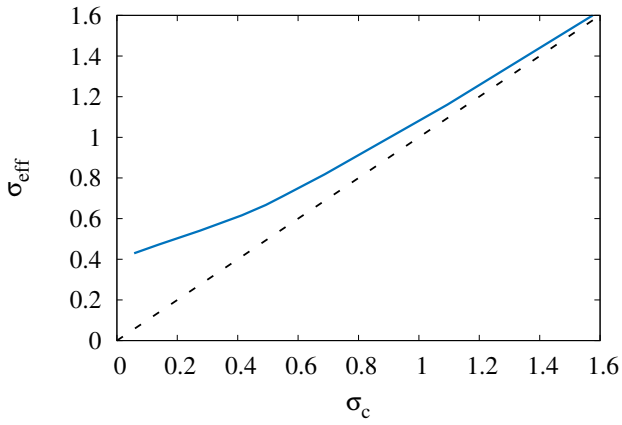

Supplementary Figure S11. Relation between the dispersion of the speckle correlation function in the original speckle and the corresponding dispersion measured in the effective speckle.

ORIENTATIONAL CORRELATIONS AND THE HEXATIC PHASE

According to KTHNY theory, two-dimensional colloidal solid phases are characterized by long-range orientational order and quasi-long-range positional order, yielding a constant orientational correlation function, $g_6(r) = \langle \phi_6^*(r_i)\phi_6(r_j)\delta(r - r_{ij})\rangle$ (with r_i the position of particle i and r_{ij} the distance between particles i and j), and a radial pair correlation function, $g(r) = \langle \delta(r - r_{ij})\rangle$, that decays as a power law with the distance [6, 7]. By contrast, the hexatic phase is characterized by quasi-long-range orientational order and short-range positional order, with an orientational correlation function that decays as a power law and a pair correlation function that decays exponentially.

To study the phase behavior of our system, we computed the orientational correlation function, $g_6(r)$. Both the experimental and numerical results are shown in the figure S12. We see that, both the experimental and numerical results suggest a hexatic phase close to the minimum of the six-fold bond order parameter and a solid phase at lower and higher values of the molar fraction. Note that, the spatial range considered here is limited by the confining potential to a maximum distance of $10\times$ times the particle diameter. We cannot discard the possibility of quasi-long-range orientational order for values of the distance larger than this value, as reported in Ref. [7].

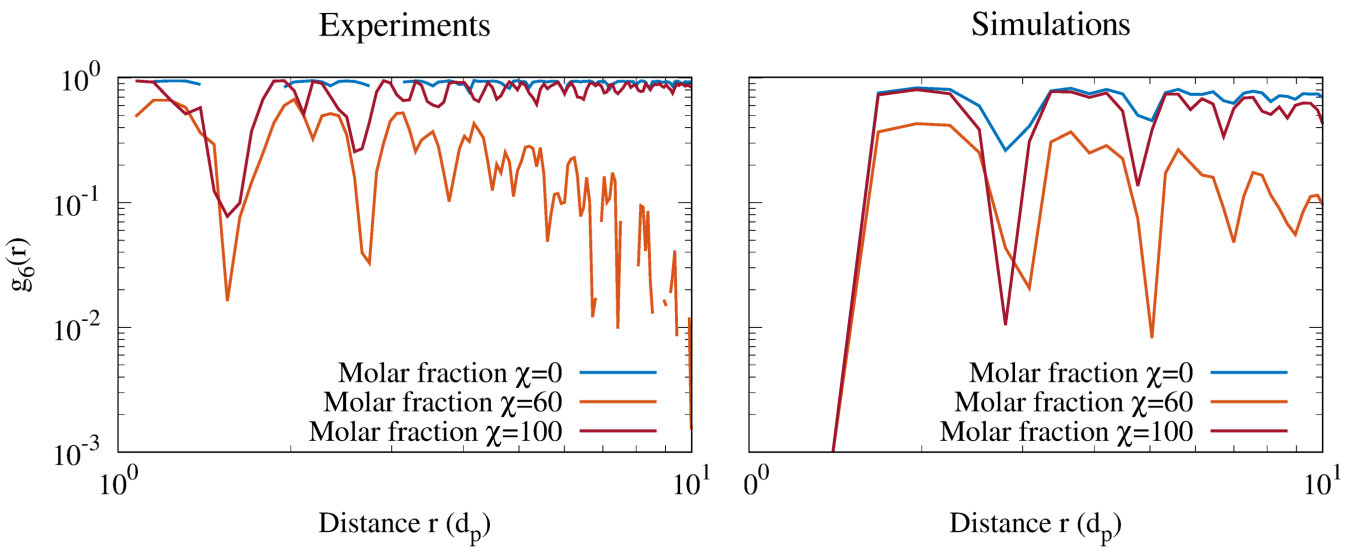

Supplementary Figure S12. Orientational correlations, $g_6(r)$, in experiments (left panel) and simulations (right panel) for different fractions of strong particles.

* contributed equally.
† nmaraujo@fc.ul.pt

[1] S. H. Behrens and D. G. Grier, "Pair interaction of charged colloidal spheres near a charged wall," Phys. Rev. E **64**, 050401 (2001).

[2] Jacob N. Israelachvili, *Intermolecular and Surface Forces*, third edition ed. (Academic Press, 2011).

[3] P. Sathyanarayana, C. Agnese, T. Yazgan, B. Lukas, D Siegfried, G. Andrea, and V. Giovanni, "Nonadditivity of critical casimir forces," Nat. Commun. **7**, 11403 (2016).

[4] L. P. García, J. D. Pérez, G. Volpe, A. V. Arzola, and G. Volpe, "High-performance reconstruction of microscopic force fields from brownian trajectories," Nat. Commun. **9** (2018).

[5] A. Callegari, M. Mijalkov, A. B. Gököz, and G. Volpe, "Computational toolbox for optical tweezers in geometrical optics," J. Opt. Soc. Am. B **32**, B11 (2015).

[6] S. C. Kapfer and W. Krauth, "Two-dimensional melting: From liquid-hexatic coexistence to continuous transitions," Phys. Rev. Lett. **114**, 035702 (2015).

[7] U. Gasser, C. Eisenmann, G. Maret, and P. Keim, "Melting of crystals in two dimensions," Chem. Phys. Chem. **11**, 963–970 (2010).